



OPEN Research on three-stage hybrid optimization control of the three-level half-bridge LLC resonant converter

Junrui Wang[✉], Jianfei Chen, Dongqi Zhao, Hao Qin & Ruiqi Li

With the rise of the charging level of new energy vehicles, the three-level half-bridge LLC topology is gradually applied to the rear stage of DC charging pile. This topology often adopts a hybrid control mode of Pulse Frequency Modulation (PFM) and Phase Shift Modulation (PSM) to obtain a wide output range. However, the PFM and PSM hybrid control can not meet the Zero Voltage Switch (ZVS) of the inner tube at the low voltage output. In order to solve this problem, this paper analyses the conditions of LLC to achieve ZVS, and proposes a Variable Frequency Burst Modulation (VFBM) to maintain dead time and minimum effective duty cycle, and forms a three-stage hybrid optimization control strategy with PSM and PFM, and sets three mode switching points to make the system work in different control modes under different output levels. Finally, the simulation model of fixed input 600 V and output 150–650 V was established by Matlab/Simulink to verify that the three-stage hybrid optimization control strategy can not only realize the inner tube ZVS in low voltage interval, but also realize the wide output voltage range, which improves the efficiency of the system. And can accurately switch the working mode, so that the post-stage system output stable, continuous and adjustable DC voltage.

Keywords Three-level half-bridge LLC, DC charging pile post stage, Variable frequency burst modulation, Three-stage hybrid optimization control, Low voltage ZVS

With the progress of economy, new energy vehicles have become a global research hotspot¹. While vigorously promoting the development of new energy vehicles industry, the development of charging piles can not be ignored. Compared with other topologies, LLC isolated topology has the advantages of high power density, simple structure and good soft switching characteristics², which is widely used in DC charging pile after stage.

Due to its unique advantages, LLC has been studied by scholars at home and abroad. In reference³, a hybrid clamp type three-level half-bridge LLC topology was used, and a two-stage hybrid control of Pulse Frequency Modulation (PFM) was used in step-up and Phase Shift Modulation (PSM) was used in step-down. However, the Zero Voltage Switch (ZVS) of the switch tube in the original edge cannot be realized at low voltage output. A off-time control strategy has been proposed in the literature⁴, and the proposed method reduces the switching and conduction losses in the low-voltage output case by skipping several pairs of switching control pulses and changes the switching frequency less than the normal control method. However, its practical control is complicated and it is difficult to design an accurate turn-off control ratio. In reference⁵, the new Burst control based on the highest efficiency phase plane trajectory was introduced into the two-level variable structure LLC topology to effectively improve the working efficiency and realize ZVS at low voltage. In reference⁶, PWM control was introduced into the bidirectional LLC topology, and the system voltage gain reached 4 times by using the switching coordination between the full bridge and half bridge of the primary side. However, there are many switches in this topology and the control is relatively complex. In reference⁷, asymmetric LLC topology is used to obtain high voltage gain in different operating modes by using the interaction of two resonators. However, the voltage gain depends on the choice of voltage mode, and the calculation of key parameters is relatively complex. Literature⁸ introduces variable PWM control in the Burst control mode with fixed frequency, so that the system can achieve ZVS while obtaining a wide voltage output range. In reference⁹, a half-bridge LLC topology with controllable resonant inductance is proposed, which can adjust the resonant inductance according to the output current to affect the parameters of the resonator, and has good dynamic performance. However, this topology requires additional magnetic adjustment structure, which leads to complex system structure and high cost. The LLC resonant

School of Electrical Information Engineering, North Minzu University, Yinchuan 750000, China. ✉email: jr09110111@163.com

converter is a nonlinear circuit, so it is necessary to simplify the circuit model when analyzing the converter. Therefore, scholars have conducted in-depth research on the solution of dynamic nonlinear equations¹⁰ and the suppression of harmonic noise^{11,12}.

For the three-level LLC topology, the inner tube is turned off later than the outer tube, so the resonant cavity current of the inner tube is less than the outer tube when the inner tube is turned off, which leads to the conditions for the soft switching of the inner tube being more stringent than the outer tube¹³. At low voltage output, the outer tube achieves ZVS but the inner tube cannot. In summary, in order to further optimize the control of LLC topology applied to the rear stage of charging pile at the low-voltage output, this paper analyzes the realization conditions of ZVS and the switching points of each mode based on the hybrid clamp half-bridge three-level LLC resonant converter, and introduces the frequency conversion burst control at the low-voltage output to realize the inner tube ZVS at the low-voltage output. Combined with PFM and PSM to form a three-stage hybrid optimization control, the latter stage of the charging pile obtains a wide output voltage range while the former stage stably supplies power and solves the problem that the inner tube can not achieve ZVS when the low voltage is output, so that the latter stage system is stable, efficient and safe.

This research can be used to reduce the energy loss in the case of low voltage output at the rear stage of DC charging piles for electric vehicles and improve the efficiency of energy transmission. This can not only reduce the use of electric energy, but also reduce the heating and wear of the internal components of the charging pile, extend the service life of the equipment, and thus reduce the operating cost of the enterprise.

Working principle of three-level half-bridge LLC resonant converter

Topology structure

The hybrid clamp topology is easier to achieve automatic midpoint voltage equalization than the topology with only clamp diodes and flying capacitors. Its circuit topology is shown Fig. 1.

In the Figure, U_i is the prestage output stable DC bus voltage; C_1 and C_2 are DC bus capacitors; D_{11} and D_{12} are clamp diodes; C_S is the flying capacitance; $Q_1 \sim Q_4$ are the primary edge switch tubes, among which Q_2 and Q_3 are the inner tubes, and the conditions for achieving ZVS are more demanding. L_r , L_m and C_r are resonant inductors, excitation inductors and resonant capacitors, which together form a resonant cavity. T is high frequency transformer; $D_{21} \sim D_{24}$ are secondary side rectifier diodes; C_o is the output filter capacitor; R_L is the load resistance.

Principle of operation

The resonant frequencies of L_r and C_r are defined as f_{r1} . The common resonant frequency of L_r , L_m and C_r is defined as f_{r2} . The operating frequency of the system is defined as f_r . In this paper, the hybrid control method of VFBM, PSM and PFM is adopted, in which the operating frequency of the system is always within $f_{r1} \sim f_{r2}$ when using PSM and PFM control. It is assumed that all components are ideal devices and the pressure bearing of the primary edge switch tube is constant at $0.5U_i$. The working principle and mode are analyzed with the system working in the subresonant state ($f_{r2} < f_r < f_{r1}$), and the main waveform is shown in Fig. 2.

In the Figure, $Q_{g1} \sim Q_{g4}$ are the driving signals, i_r and i_m are the current values flowing through the resonant inductor and excitation inductor, $i_{D21} \sim i_{D24}$ are the secondary side diode current. The converter has eight operating modes in one cycle, and only the first half cycle is analyzed in this paper because the resonant state is the same before and after half cycle.

Working mode 1: Working phase ($t_0 \sim t_1$). Q_1 is conducting at the same time as Q_2 at time t_0 , and since D_{21} and D_{24} are already conducting at this time, the voltage will clamp the L_m at this time, and the L_m will not participate in the resonance. At this time, L_r and C_r participate in the resonance, and the current flows through Q_1 , Q_2 , L_r , C_r and C_1 , and i_m rises linearly.

Working mode 2: Working phase ($t_1 \sim t_2$). i_r is equal to i_m at time t_1 , at which time D_{21} and D_{24} achieve zero-current turn-off. At this time, the primary edge of the converter enters the reactive power circulation phase, and the L_m is no longer clamped and resonates with L_r and C_r . Since L_m is generally 5 to 7 times larger than L_r , the current i_r flowing through the resonant inductor can be approximately considered constant.

Working mode 3: Working phase ($t_2 \sim t_3$). Q_1 is turned off at time t_2 , and the i_r will charge the parasitic capacitance to Q_1 to $0.5U_i$. At the same time i_r discharges the parasitic capacitor voltage of Q_4 to 0 through C_S to

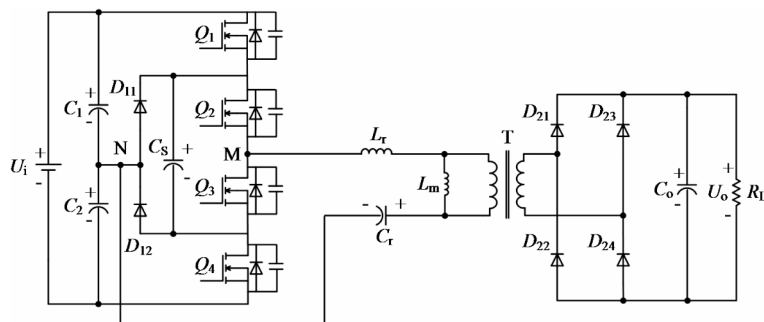


Fig. 1. Three-level half-bridge hybrid clamp type LLC topology.

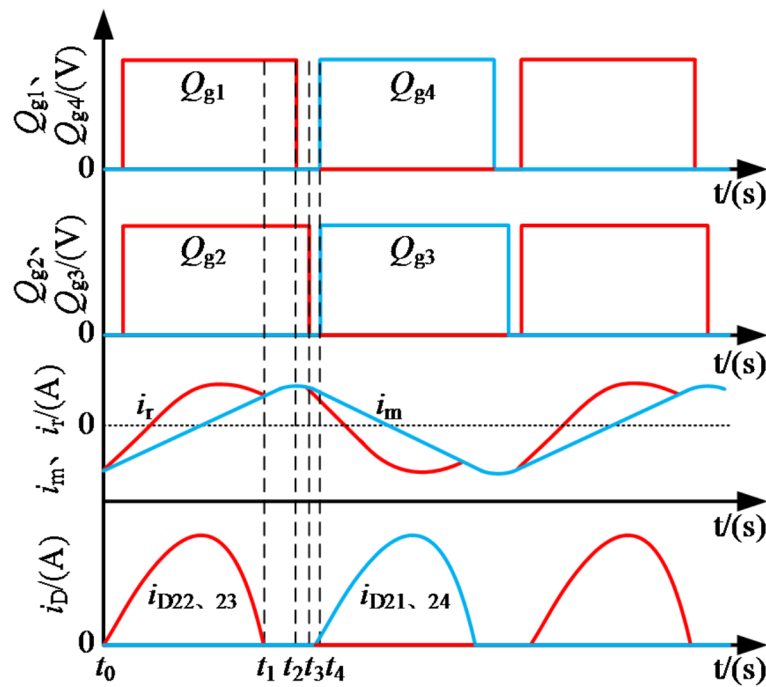


Fig. 2. Subresonant waveform.

prepare for Q_4 's ZVS. Finally, the upper clamp diode D_{11} clamps the Q_1 voltage to $0.5U_i$, at which point the loop through which the resonant inductor i_r flows is D_{11} , Q_2 , L_m and C_r .

Working mode 4: Working phase ($t_3 \sim t_4$). Q_2 is turned off at time t_3 , and the i_r will charge the parasitic capacitance of Q_2 to $0.5U_i$. At the same time i_r discharges the parasitic capacitor voltage of Q_3 to 0, creating conditions for the ZVS of Q_3 . Eventually, the inductor current i_r flows through D_{24} , D_{23} , L_r , L_m and C_r . After Q_2 is turned off, the secondary side diodes D_{22} and D_{23} conduction, L_m reverse clamp, i_m starts to linearly decrease. ZVS is realized simultaneously at time Q_3 and Q_4 of t_4 .

Here, the other state of the system is working in the resonant state ($f_r = f_{r1}$), and the main waveform is shown in Fig. 3.

As can be seen from Fig. 3, the resonant cavity current is a standard sine wave, L_m does not participate in the resonance, i_m waveform is a triangle wave, secondary side diode is in the critical state of ZCS. At this time, the switching frequency f_r is consistent with the resonant frequency f_{r1} of L_r and C_r , the output voltage is only determined by the input and the number of transformer turns, and the efficiency of the converter is the highest.

Effective duty cycle is the ratio of the time that the periodic signal is in effective state to the entire cycle time in a cycle. PSM control controls the actual effective duty cycle D of the inverter output voltage by controlling the phase shift Angle between the leading tube and the lagging tube, so as to change the actual effective value of the inverter output voltage. The system is in the PSM control working waveform as shown in Fig. 4.

Analysis of limitations of two-stage hybrid control ZVS

Dead time is a period of safety interval set to prevent the phenomenon of short-circuiting caused by the simultaneous conduction of two switching elements (e.g., MOSFETs or IGBTs) on the same bridge arm. In other words, dead time means that after one tube is closed, a certain amount of time must be waited before the other tube can be opened. In light load and low voltage output state, too short dead time may cause ZVS to fail, while too long dead time will cause the resonant current to reverse resonance to re-charge the parasitic capacitor and cause ZVS to fail. According to the analysis in Sect. 2.2, the system should work in the sub-resonant region to ensure the primary edge ZVS and secondary edge ZCS, so the PSM should be switched during the step-down output. In the PSM working state, the system operating frequency should always meet $f_r = f_{r1}$ while achieving ZVS, and reasonable dead time T_d and effective duty cycle D should be calculated. In the following, the derivation of the dead time when the switching frequency is equal to the resonant frequency is first carried out, and the resonant frequency current waveform is shown in Fig. 5.

Let the time interval for the resonant current to change from reverse to 0 be θ , then the expression of the dead time T_d at this time can be expressed as:

$$T_d = \frac{\theta}{\omega_s} \quad (1)$$

Where ω_s is the system resonant frequency angular velocity. The instantaneous values of resonant current and excitation current in the Figure can be expressed as:

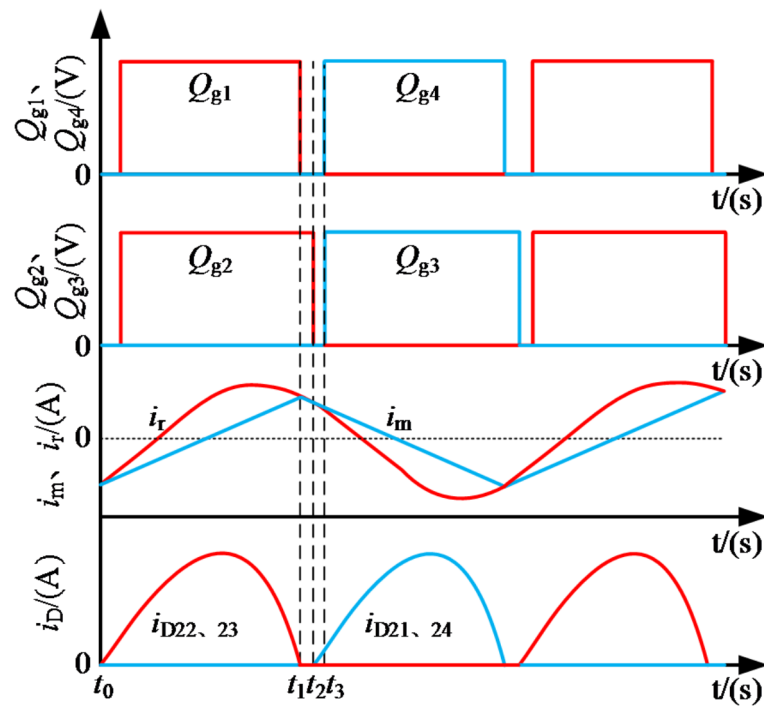


Fig. 3. Resonant state waveform.

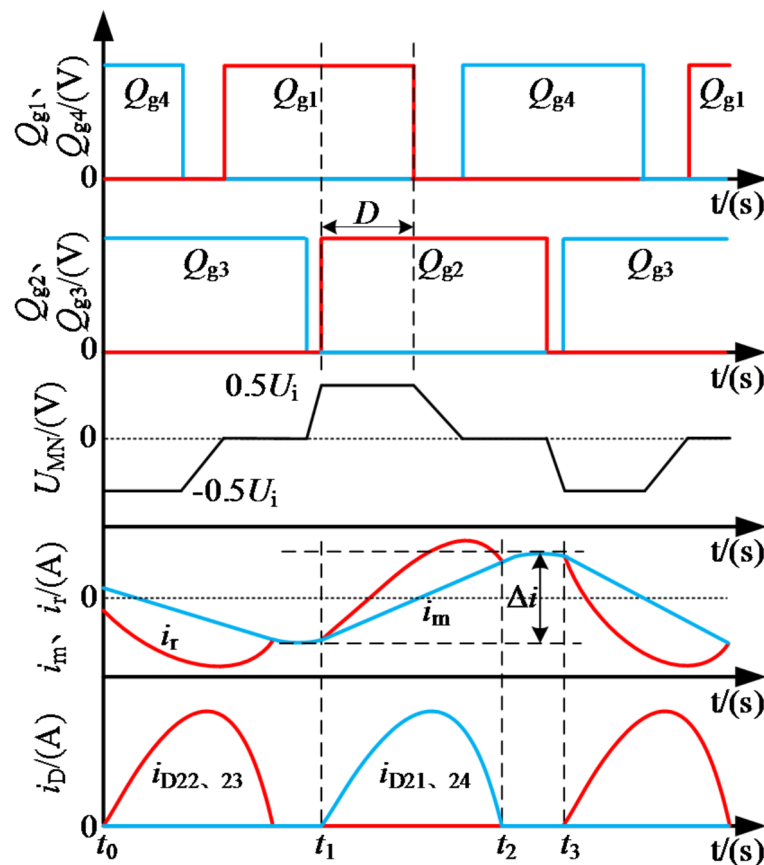


Fig. 4. PSM working waveform.

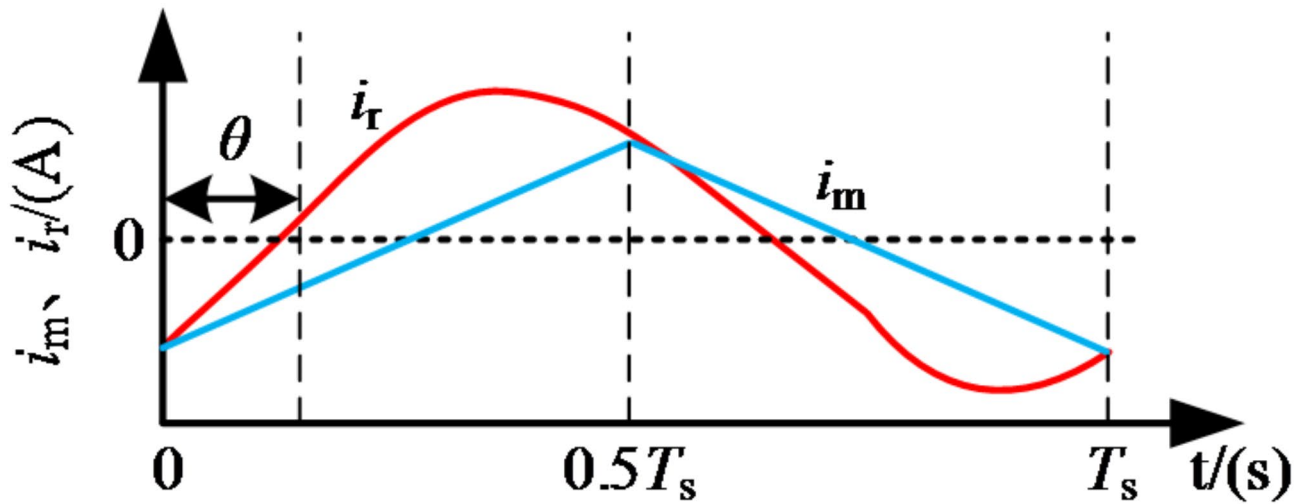


Fig. 5. Resonant frequency current waveform.

$$i_r(t) = \sqrt{2}i_{r_rms} \sin(\omega t - \theta) \quad (2)$$

$$i_m(t) = \begin{cases} \frac{n_2 \cdot U_o t}{L_m} - i_{m_max} & 0 < t < 0.5T_s \\ -(\frac{n_2 \cdot U_o t}{L_m} - i_{m_max}) & 0.5T_s < t < T_s \end{cases} \quad (3)$$

Where $n_2 = 1/n$ is the conversion ratio to the original edge and T_s is the system period. Suppose that the expression i_{m_max} is given by:

$$i_{m_max} = \frac{n_2 \cdot U_o}{4f_r L_m} \quad (4)$$

Since the resonant energy of the secondary edge comes from the integral of the difference between the resonant current of the primary edge and the excitation current, the effective value of the resonant current can be obtained as:

$$i_{r_rms} = \sqrt{\frac{(4L_m^2 \pi^2 f_r^2 + n_2^4 R_L^2) U_o^2}{8n_2^2 R_L^2 f_r^2 L_m^2}} \quad (5)$$

According Fig. 5, the initial value expression of the resonant current is:

$$i_r(t)_{t=0} = \sqrt{2}i_{r_rms} \sin(-\theta) = -\frac{n_2 \cdot U_o}{4f_r L_m} \quad (6)$$

By substituting Eq. (5) into Eq. (6), the expression of time interval θ can be obtained as:

$$\theta = \arcsin\left(\frac{n_2 U_o}{\sqrt{\frac{4U_o^2 (4L_m^2 \pi^2 f_r^2 + n_2^4 R_L^2)}{n_2^2 R_L^2}}}\right) \quad (7)$$

The maximum value of the dead time T_d can be obtained by substituting Eq. (7) into Eq. (1), which is denoted as T_{d_max} . In theory, ZVS can be achieved if the dead time can satisfy one charge and discharge of the parasitic capacitance C_{oss} of the switch tube, denoted as T_{d_min} , and its expression is:

$$T_{d_min} = \frac{0.5U_i C_{oss}}{i_{m_max}} \quad (8)$$

In conclusion, when the switching frequency of the system is the resonant frequency point, the dead time should meet Eqs. (1) and (7). However, when the PSM control is used, not only the dead time should be considered, but also the ZVS condition is related to the effective duty cycle. In order to ensure that the resonant current of the inner tube Q_2 and Q_3 can still charge and discharge the parasitic capacitance in the dead time, The minimum effective duty cycle must be calculated.

Figure 4 shows that the dead time T_d is within $t_2 \sim t_3$, but the mathematical expression of i_r is complicated to solve. Since $i_r = i_m$ when $t_2 \sim t_3$, i_r can be represented by i_m in the dead time, where the rate of change of i_m can be expressed as:

$$\Delta i = \frac{nU_oD}{2f_rL_m} \tag{9}$$

The amplitude of i_m at the maximum point is given by:

$$i_m = 0.5\Delta i \geq \frac{2C_{oss}U_{C1}}{T_d} \tag{10}$$

Combined with Eqs. (9) and (10), the minimum effective duty cycle can be obtained as:

$$D_{min} \geq \frac{8C_{oss}U_{C1}f_rL_m}{nU_oT_d} \tag{11}$$

In summary, in the PFM and PSM (PFM-PSM) hybrid control, Eqs. (1), (7), and (11) need to be satisfied at the same time to make the original edge switch tube ZVS. The key parameters of the existing converter are shown in Table 1.

Substitute the parameters into Eqs. (1) and (7), and the dead time range is $2.7\text{e-}9\text{s} \leq T_d \leq 6.73\text{e-}7\text{s}$. When the dead time is less than the minimum value, the parasitic capacitor cannot achieve primary charge and discharge, resulting in the inability to achieve inner tube ZVS. When the dead time is greater than the maximum value, the resonant current will reverse resonance after zero-crossing, resulting in reverse charging of the parasitic capacitor that has been discharged. ZVS could not be implemented. In summary, the dead time $T_d = 3\text{e-}8\text{s}$ is selected in this paper, and the minimum output voltage value of 150 V is substituted into Eq. (11) to obtain the minimum effective duty cycle $D_{min} \geq 0.44$, and the gain is $M_{PSM} = 0.637$ at this time, that is, ZVS cannot be realized below this gain. Combined with Table 1, it can be seen that the minimum ZVS voltage achieved under this gain is 299.6 V, not the minimum output voltage of 150 V, and the full output voltage range of ZVS cannot be achieved. Taking the output of 250 V under the condition of Table 1 as an example, the main waveform is shown in Fig. 6. It can be seen that in the PFM-PSM hybrid control, The phenomenon of ZVS failure in PSM operation mode, so it is necessary to optimize the voltage interval from 150 V to 300 V.

Three-stage hybrid optimization control strategy

In order to solve the problem that ZVS cannot be realized and work efficiency is low at low voltage, some scholars have proposed burst mode to reduce energy loss by blocking the driving signal of the switch tube. Literature¹⁴ proposed a hybrid control method based on PFM-burst to improve the working efficiency of the LLC converter in the full voltage range, aiming at the problem that the LLC converter is difficult to adjust under the condition of very light load and no load. In reference¹⁵, a phase-shift burst modulation (PS-burst) method for two-level half-bridge LCC resonant converter was proposed and applied in photovoltaic system to achieve maximum power tracking while achieving full voltage range ZVS. In reference¹⁶, the charge is normalized by the switching frequency to obtain the approximate linear relationship between the charge and the load current, and the current sensorless burst control of the half-bridge LLC converter is proposed. Literature¹⁷ proposed a PSM-burst hybrid control mode based on two-level full-bridge LLC converter, which achieved wide output voltage range, low resonant current and zero-voltage turn-on of all switches, and optimized resonant parameters and maximum phase shift Angle. Literature¹⁸ combined with adaptive theory on the basis of burst control, so that the burst frequency was kept at the preset frequency and the resonant tank operated at the preset optimal load point during the burst time, which solved the problems of current overshoot and low efficiency in traditional burst mode. Drawing on the above control ideas, this paper proposes a burst control of continuous frequency conversion, namely VFBS, which adjusts the output voltage and current of the converter through closed-loop control of the burst period. As the output voltage increases, the burst period also increases. The main working waveform is shown Fig. 7.

It can be seen from Fig. 7 that the driving state in the VFBS is high and low alternately at this time. When the first pulse ends, the switch tube can still be charged and discharged in the dead time, which meets the ZVS

System parameters	Parameter values
Input voltage U_i	600 V
Output voltage U_o	150 ~ 650 V
Frequency of resonance f_r	120 kHz
Resonant inductance L_r	8e-6 H
Resonant capacitance C_r	220e-9 F
Parasitic capacitance C_{oss}	1e-10 F
Ratio of inductance k	0.182
Factor of quality Q	0.32
Ratio of change n	0.64
PFM-PSM switching point U_{s1}	470 V
Resistance of load R_L	56.03Ω

Table 1. Key parameters of the converter.

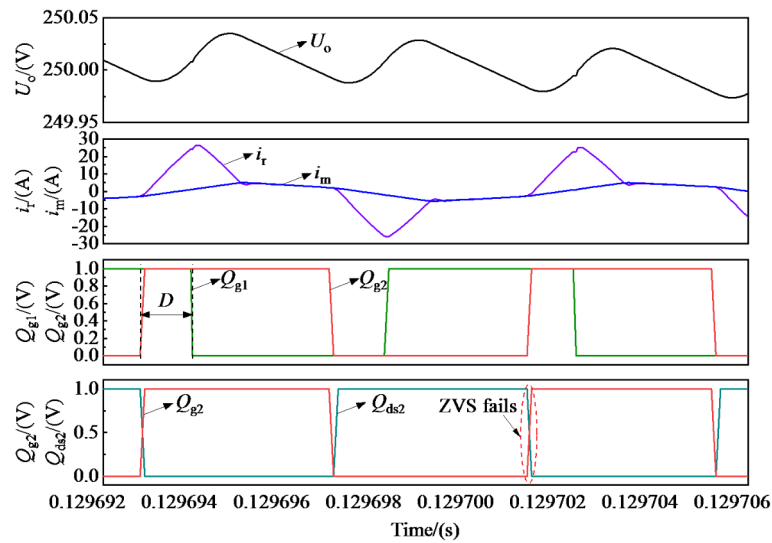


Fig. 6. The main waveform diagram of output 250 V in PSM operating mode.

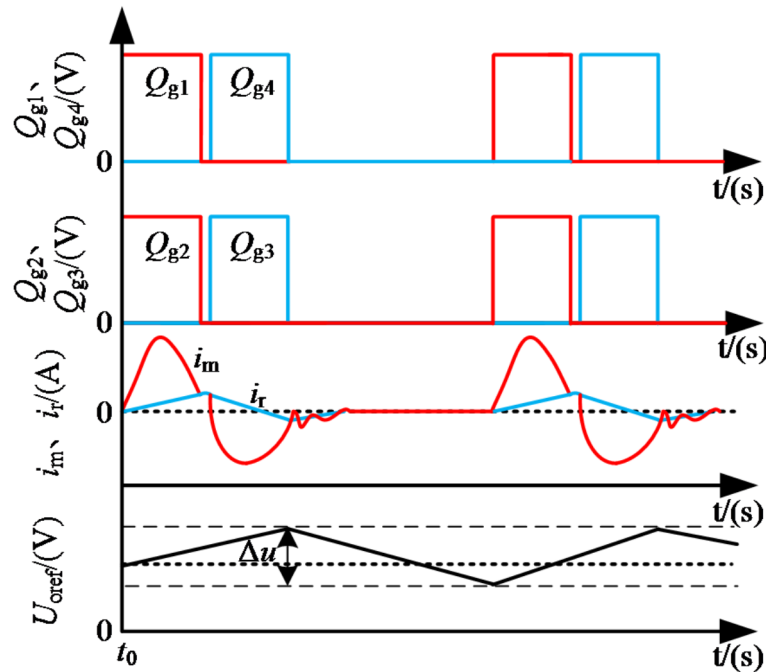


Fig. 7. VFBM working waveform.

condition. Combined with the previous analysis, the minimum effective duty cycle is introduced on this basis to prevent the output voltage fluctuation at the switching point. The three-stage hybrid optimization control was composed by VFBM and PSM and PFM. The switching point between VFBM and PSM was defined as the first switching point and set to 300 V, the switching point between PSM and PFM was defined as the second switching point and set to 470 V, and the system operating frequency under VFBM mode was defined as f_{burst} . The gain curve of the three-stage hybrid optimization control is shown in Fig. 8. Since the system needs to judge different voltage ranges according to the charging demand of the power battery in the actual work, the frequency conversion burst control is recorded as Mode1, PSM control as Mode2, and PFM mode as Mode3.

When the output voltage increases, f_{burst} increases, and the output gain also increases. When the gain is 0.637, that is, the output voltage is 300 V, the system switches to PSM control. At this time, the system works at the resonant frequency, and the effective duty cycle increases with the increase of the output voltage. When the output voltage is 470 V, that is, when the gain is 1, the maximum effective duty cycle is also 1. The system is in the resonant frequency state, and the excitation current is independent of the load. When the output voltage continues to increase, the system works under the control of PFM, and the normalized frequency continues to

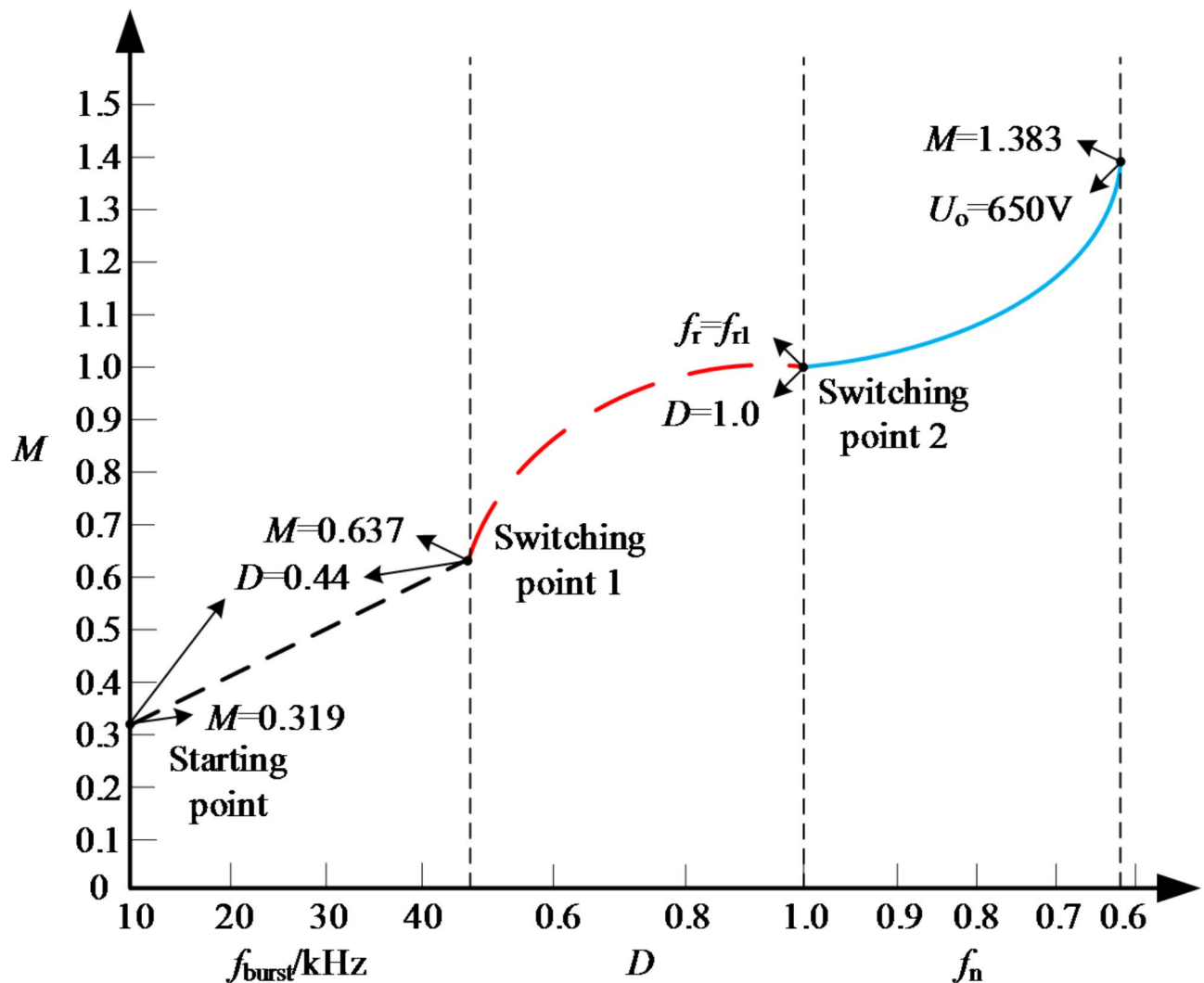


Fig. 8. Three stage gain curve.

decrease. When the output voltage is 650 V, the system reaches the maximum gain, which is 1.383, less than the maximum gain of 1.58 when L_r, L_m, C_r , and common resonance $f_r = f_{r2}$. Since different voltage intervals need to be judged in the actual work of the system, the VFBM is denoted as Mode1, PSM control as Mode2, and PFM mode as Mode3. The working flow of the system is shown in Fig. 9.

Simulation experiment verification

In order to verify the correctness of the proposed three-stage hybrid optimization control strategy, this paper builds a simulation model in Matlab/Simulink, and the key parameters of the system are given in Table 1. 300 V and 470 V are selected as the mode switching points, and the three modes of Mode1, 2 and 3 are simulated and analyzed respectively.

Verification by Mode1 simulation

In Mode1, the system starts working with an output voltage of 150 V and a gain of 0.319, and the maximum output voltage in this mode is 300 V. The main waveforms of the system at the output voltage of 150 V and 300 V are shown in Figs. 10 and 11. Figure 10 shows that $\Delta u = 0.7V$, and the minimum effective duty cycle of Q_2, Q_3, Q_1, Q_4 is D_{\min} , at this time f_{burst} is 14.3 kHz. Figure 11 shows that the system still maintains the minimum effective duty cycle, at this time f_{burst} is 54.1 kHz, $\Delta u = 0.45V$. In this state, taking inner tube Q_2 as an example, the ZVS waveform at 150 V and 300 V output is shown in Figs. 12 and 13, where the drain-source voltage of Q_2 has been reduced by 300 times in equal proportion for convenient display.

In conclusion, it can be seen that under the control of VFBM, f_{burst} of the system increases with the increase of output voltage, and Q_2, Q_3, Q_1 and Q_4 always maintain the minimum effective duty cycle D_{\min} . Simulation experiments show that the control strategy can achieve stable output while meeting the Q_2 ZVS of the inner tube, which verifies the correctness of the VFBM strategy.

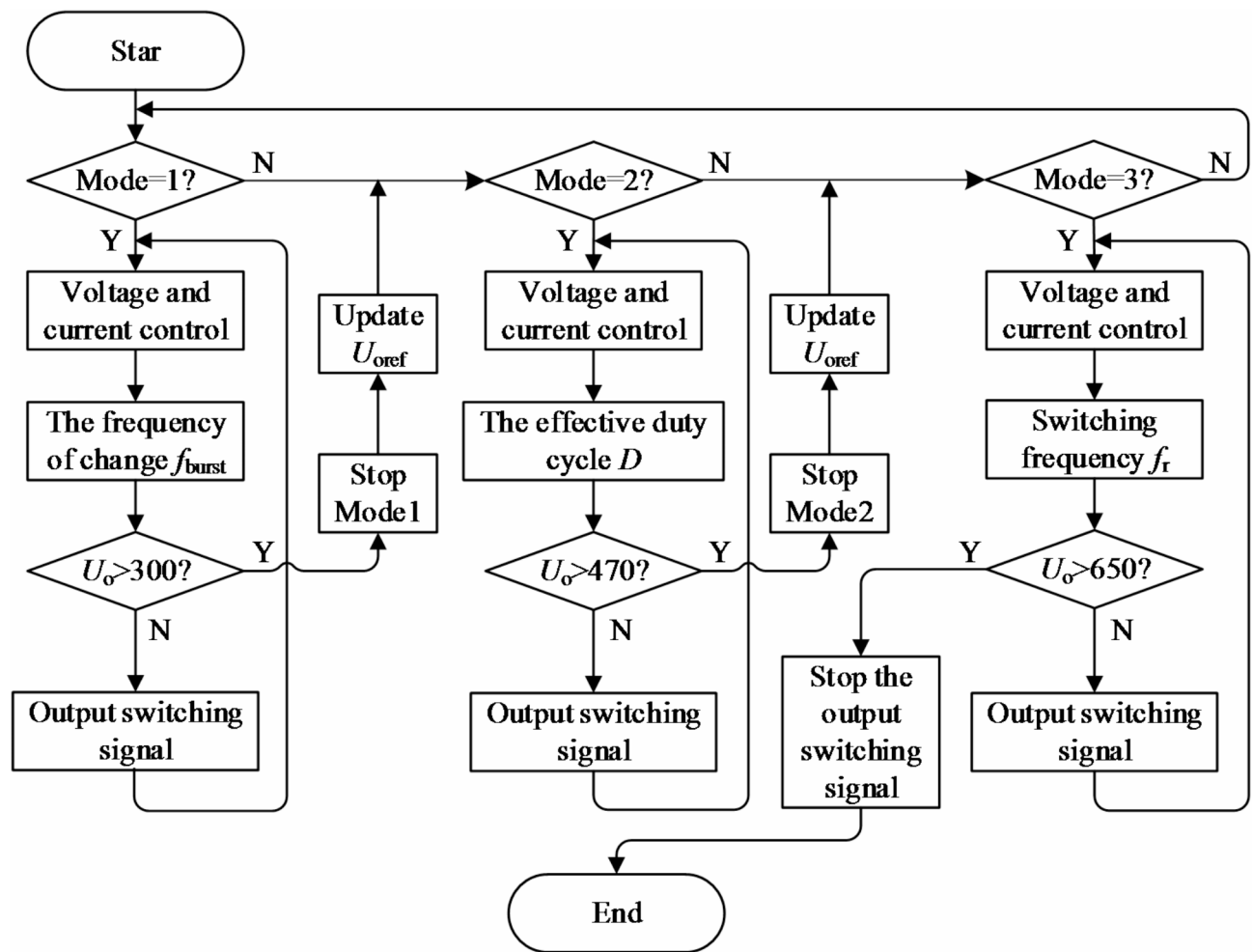


Fig. 9. System flow chart.

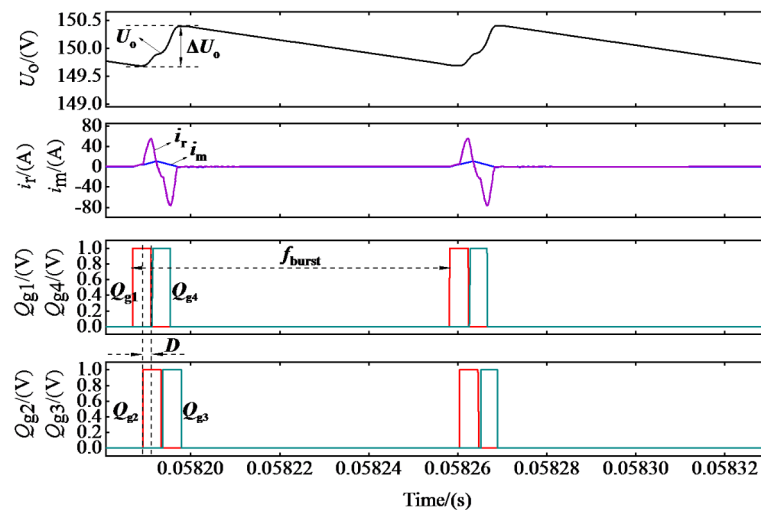


Fig. 10. Main waveform diagram of output 150 V in VFBL.

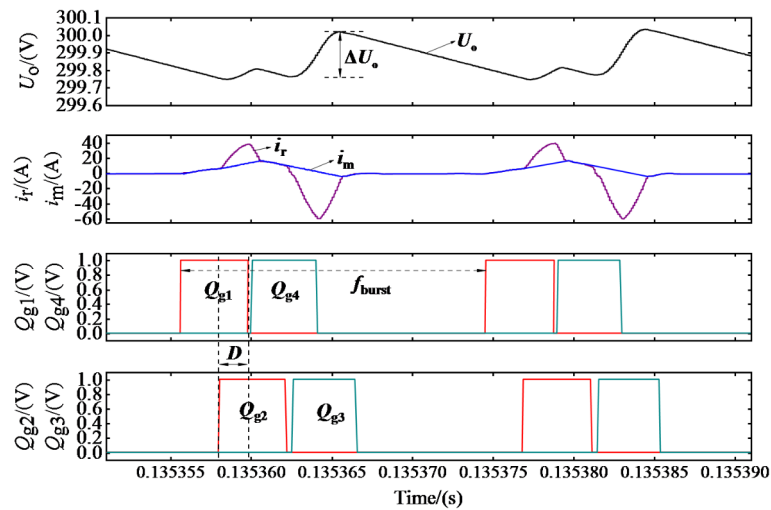


Fig. 11. Main waveform diagram of output 300 V in VFBL.

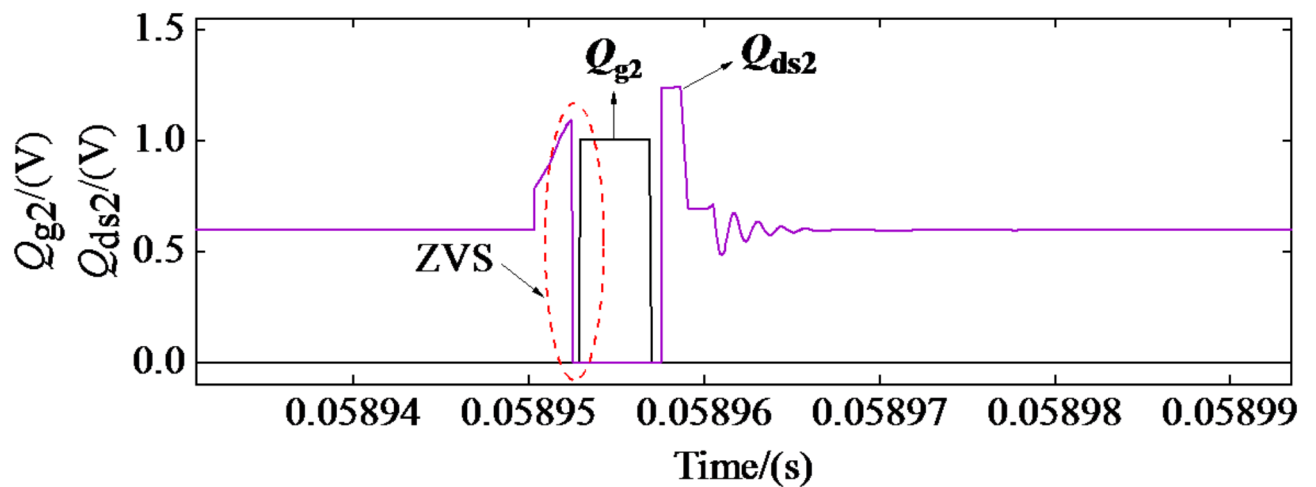


Fig. 12. Q_2 tube ZVS waveform at output voltage of 150 V.

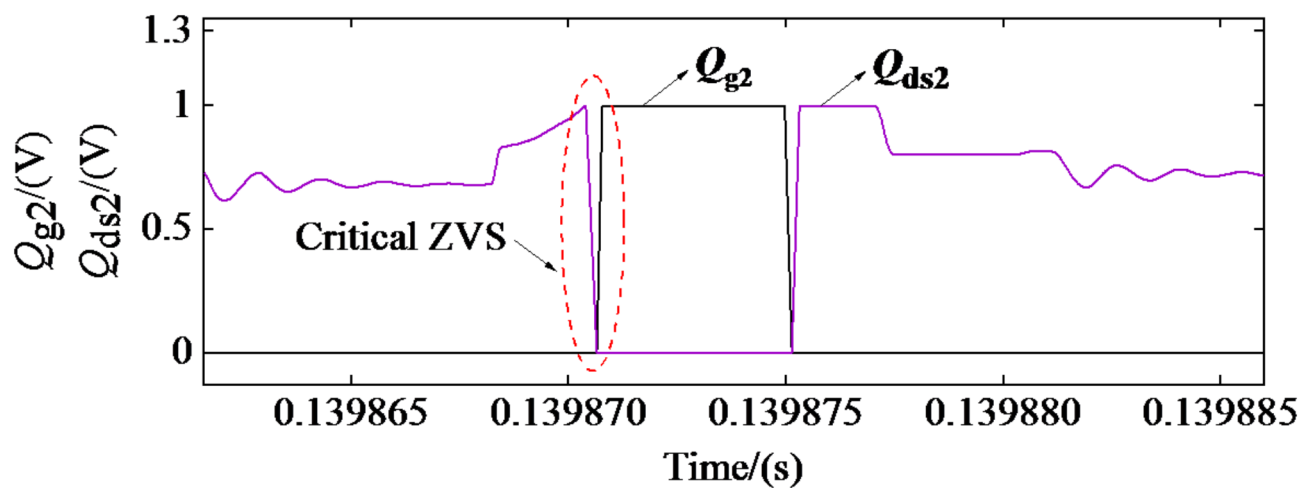


Fig. 13. Q_2 tube ZVS waveform at output voltage of 300 V.

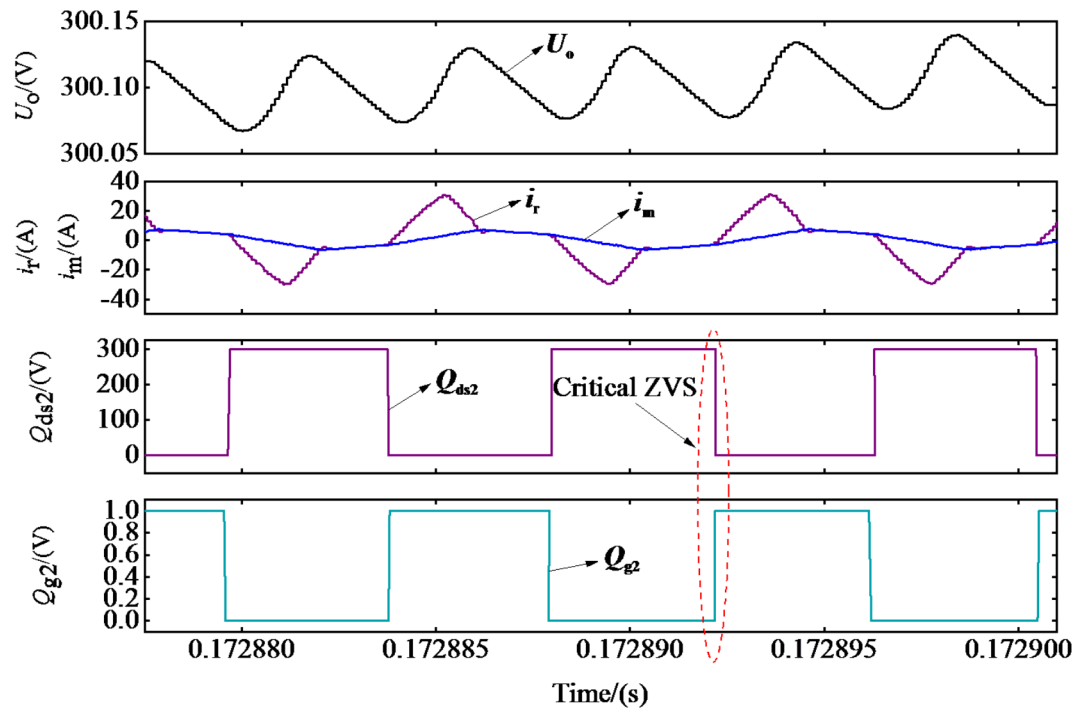


Fig. 14. Main waveform diagram of output 300 V in PSM.

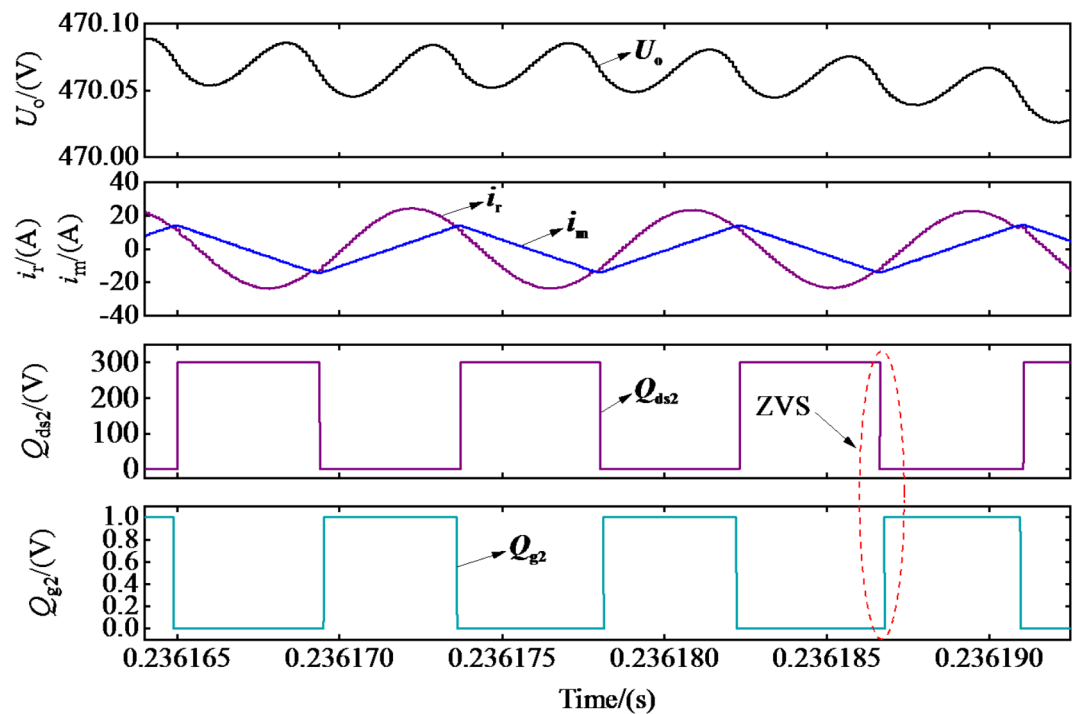


Fig. 15. The main waveform of the resonant frequency point.

Verification by Mode2 simulation

In Mode2, the output voltage of the system ranges from 300 V to 470 V, and the system starts to work with gain 0.637 until gain 1. In this mode, the system resonant frequency $f_r = f_{r1}$. The main waveform is shown in Fig. 14, and it can be seen that the Q_{2s} is in the critical ZVS state at this time.

In this paper, the output voltage is 470 V and the gain is 1, so the system works at the resonant frequency point, and the main waveform is shown in Fig. 15.

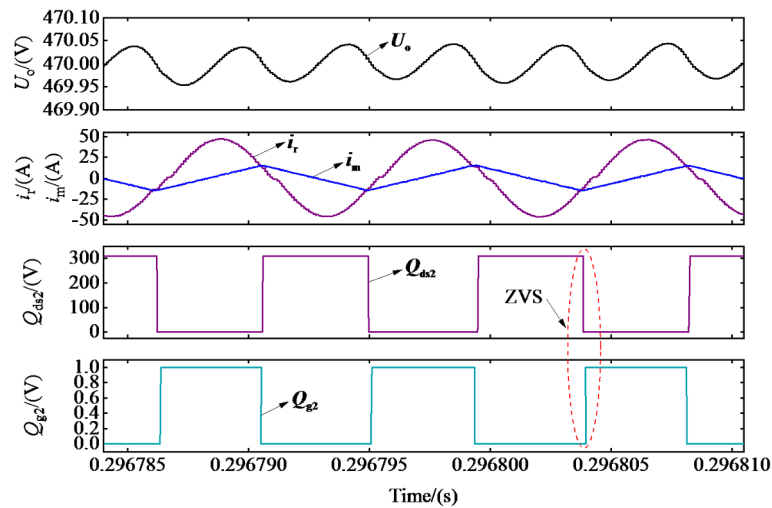


Fig. 16. Main waveform diagram of PFM at resonant frequency.

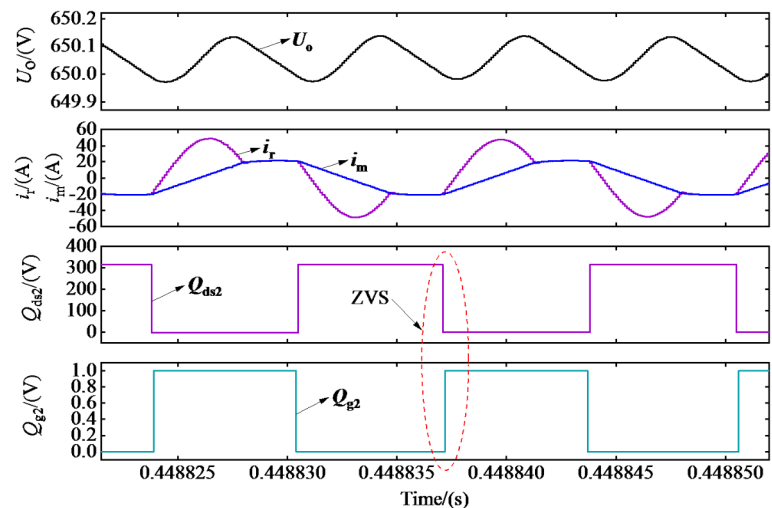


Fig. 17. Main waveform diagram of output 650 V in PFM.

Verification by Mode3 simulation

In Mode3, the system starts working with $f_n = 1$ with output voltage ranging from 470 V to 650 V.

Figure 15 shows that the resonant current is approximately a sine wave, the excitation current is approximately a triangle wave, the output voltage is stable, and Q_2 can achieve ZVS. In summary, the correctness of the PSM control strategy is verified, and the simulation results show that the control strategy can achieve stable output and meet the ZVS of the inner tube.

In order to verify the working characteristics of the resonant frequency point under PFM, it is merged into R_L when it is stable, and the total resistance is 28.015Ω . The waveform after loading at the resonant frequency point is shown in Fig. 16. When the output voltage exceeds 470 V, the system resonant frequency $f_{r2} < f_r < f_{r1}$, working in subresonant mode, the full-voltage output waveform of the system is shown in Fig. 17.

Figure 16 shows that the resonant current and excitation current only change in amplitude after the load is cut, and the working waveform is similar to that without load cut. The stable output is achieved and the inner switching tube ZVS is satisfied, which verifies that the resonant and excitation current will not be distorted by the load when the system works at the resonant frequency. Figure 17 shows that the system operating frequency f_r is 75 kHz and the internal switching tube ZVS, and the output voltage is stable. In conclusion, the correctness of PFM modulation strategy is verified. Finally, the total output voltage waveform diagram of the three-stage hybrid optimization control is shown in Fig. 18.

As can be seen from Fig. 18, the system starts in the mode of Model1 and enters the VFBM mode, reaches 150 V in 0.06s and remains stable, changes the output voltage command to 300 V in 0.1s and reaches stability in 0.12s. Combined with Figs. 10, 11 and 12, and 13, it can be seen that in this working mode, the system output remains stable and the inner switch tube achieves ZVS, and the minimum effective duty cycle D derived

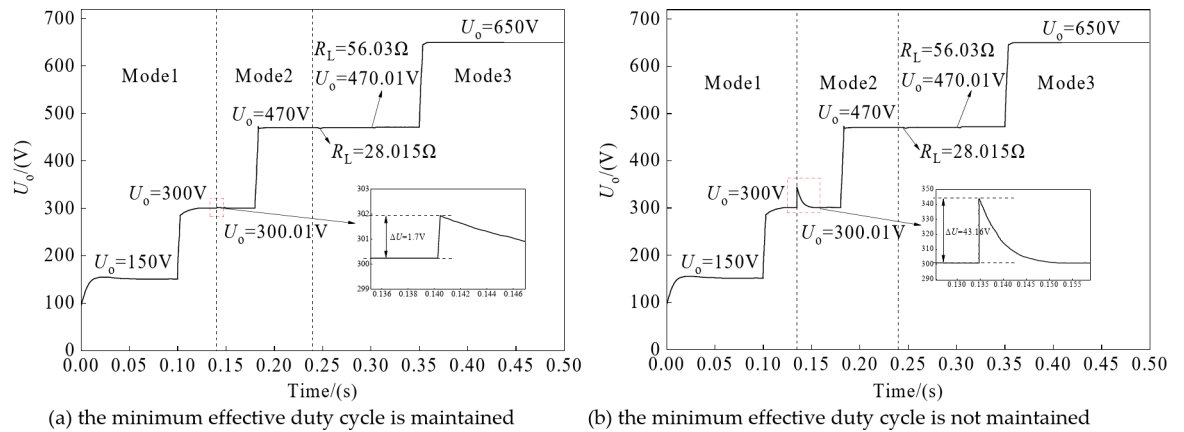


Fig. 18. Total output voltage waveform of three-stage hybrid control.

in Subsection 2.3 is maintained to enter the Mode2-PSM working mode at 0.14s. Since Figure (a) maintains the minimum duty cycle in the mode switching, Figure (a) maintains the minimum duty cycle in the mode switching. During mode switching, the voltage fluctuation is only 1.7 V, while the voltage fluctuation in Figure (b) is 43.16 V. At 0.15s, the system completely enters PSM working mode and remains stable. At this time, the system working frequency is equal to the resonant frequency of the two components. At 0.18s, the output voltage command is changed to 470 V and reaches stability at 0.19s, until it enters Mode3-PFM working mode at 0.24s. According to Figs. 14 and 15, ZVS can be realized by switching the tube within the PSM operating mode and resonant frequency point. The system carries out the load cut experiment at 0.245s, and the load is 28.015Ω at this time, and the load cut experiment restores 58Ω at 0.3s. The working characteristics of the LLC converter at the resonant frequency point are verified, and the output voltage instruction is changed to 650 V to maintain a stable output at 0.35s. Figures 16 and 17 show that ZVS is achieved by inner switching tube in PFM operating mode.

Finally, through the simulation verification of the three modes, it is proved that the three-stage hybrid optimization control strategy can achieve the full output voltage ZVS while meeting the wide output voltage range, and strictly meet the gain curve of Fig. 8.

Conclusions

Aiming at the problem that the PFM-PSM hybrid control can not meet the ZVS of the inner tube at the low voltage output, the minimum effective duty cycle and dead time are calculated on the basis of PFM-PSM, and the VFBM is introduced at the low voltage output to form a three-stage hybrid optimization control.

Theoretical and simulation results show that the three-stage hybrid optimization control can make the charging pile back stage output stable DC voltage when the front stage power supply is stable and solve the problem that the inner tube can not achieve ZVS when the low voltage output is under the PFM-PSM hybrid control. Because of the dead time and the minimum effective duty cycle in the VFBM, The voltage oscillation between VFBM and PSM is effectively suppressed. Finally, the system can realize the full range of 150 V ~ 650 V ZVS. By reasonably selecting the mode switching point and system parameters, the system can select the working mode through the required output voltage, so that the charging pile is stable, efficient and safe.

Data availability

The data used to support the findings of this study are included in the article.

Received: 13 October 2024; Accepted: 3 March 2025

Published online: 21 March 2025

References

- Wang, T., Deng, T. Y. & Peng, Y. X. Analysis of research hotspot of new energy vehicle industry based on CiteSpace. *Technol. Econ.* **39**(05), 134–141 (2020).
- Li, Z. X. et al. Research review of power electronic transformer technologies. In *Proceedings of the CSEE*. Vol. 38, no. 05, 1274–1289 (2018).
- Hu, C. G. et al. Hybrid control strategy of three-level half bridge LLC converter with wide input voltage range. *Electr. Machines Control*, 1–10 (2023).
- Yoon, H. Y., Lee, H. S., Ham, S. H., Choe, H. J. & Kang, B. Off-time control of LLC resonant half-bridge converter to prevent audible noise generation under a light-load condition. *IEEE Trans. Power Electron.* **33**(10), 8808–8817 <https://doi.org/10.1109/TPEL.2017.2774840> (2018).
- Li, Z. J. et al. *Acta Energetica Solaris Sinica*, **42**(02), 338–345 (2021).
- Zhao, Q. L. et al. Bidirectional LLC resonant converter with PWM control. *Power Syst. Technol.* **46**(05), 1990–1999 (2022).
- Zhang, J. et al. An asymmetric multi-mode LLC resonant converter with limited FM range for wide output voltage range application. *Electr. Mach. Control* 1–8. <http://kns.cnki.net/kcms/detail/23.1408.TM.20230531.1131.018.html> (2023).
- Shi, L., Liu, B. Y. & Duan, S. X. A Burst-PWM hybrid control method for wide output voltage range of LLC converter. *Trans. China Electrotechnical Soc.* **34**(22), 4772–4780 (2019).

9. Lin, W. M. et al. Half-bridge LLC circuit with controllable resonant inductor and its control method. *Electr. Machines Control*. **25**(09), 46–60 (2021).
10. Li, W., Xiao, L. & Liao, B. A Finite-Time convergent and Noise-Rejection recurrent neural network and its discretization for dynamic nonlinear equations solving. *IEEE Trans. Cybern.* **50**(7), 3195–3207. <https://doi.org/10.1109/TCYB.2019.2906263> (2020).
11. Liao, B., Wang, Y., Li, J., Guo, D. & He, Y. Harmonic noise-tolerant ZNN for dynamic matrix pseudoinversion and its application to robot manipulator. *Front. Neurobot.* **16**, 928636. <https://doi.org/10.3389/fnbot.2022.928636> (2022).
12. Xiang, Q. et al. Discrete-time noise-tolerant Zhang neural network for dynamic matrix pseudoinversion. *Soft Comput.* **23**, 755–766. <https://doi.org/10.1007/s00500-018-3119-8> (2019).
13. Meng, T. *Research and Design of Three Level Charging Pile* (Harbin Institute Of Technology, 2018).
14. Rao, G. & Zhang, Z. LLC resonant converter based on PFM-Burst hybrid control. In *MEMAT 2022; 2nd International Conference on Mechanical Engineering, Intelligent Manufacturing and Automation Technology, Guilin, China*, 1–5. (2022).
15. Chen, X., Tayebi, S. M. & Batarseh, I. Efficiency improvement of a dual-input LLC converter for PV applications using burst-mode control strategy. In *IEEE Energy Conversion Congress and Exposition (ECCE), Baltimore, MD, USA*, 6487–6494 (2019).
16. Xu, Q. et al. A charge normalization based burst mode control strategy for the LLC converter without current Sensing. *IEEE Trans. Power Electron.* **38** (9), 10623–10628 (2023).
17. Shi, L., Liu, B. & Duan, S. Burst-mode and phase-shift hybrid control method of LLC converters for wide output range applications. *IEEE Trans. Industr. Electron.* **67**(2), 1013–1023 (2020).
18. Jiang, W. et al. Constant burst frequency control for LLC converters with trajectory control. In *2018 IEEE Energy Conversion Congress and (ECCE), Portland, OR*, 6804–6808. (2018).

Author contributions

Conceptualization, J.W. and J.C.; methodology, J.W.; software, J.C.; validation, D.Z., H.Q. and R.L.; formal analysis, D.Z.; investigation, J.W.; resources, J.W.; data curation, J.C.; writing—original draft preparation, J.C.; writing—review and editing, J.W.; visualization, J.C.; supervision, J.W.; project administration, J.W.; funding acquisition, J.W. All authors have read and agreed to the published version of the manuscript.

Funding

This work was supported by the National Natural Science Foundation of China (NO. 52167004), the Natural Science Foundation of Ningxia (NO. 2024AAC03182) and the Ningxia Hui Autonomous Region Intelligent Equipment and Precision Testing Technology Research and Application Innovation Team (NO. 2022BSB03104).

Declarations

Competing interests

The authors declare no competing interests.

Additional information

Correspondence and requests for materials should be addressed to J.W.

Reprints and permissions information is available at www.nature.com/reprints.

Publisher's note Springer Nature remains neutral with regard to jurisdictional claims in published maps and institutional affiliations.

Open Access This article is licensed under a Creative Commons Attribution-NonCommercial-NoDerivatives 4.0 International License, which permits any non-commercial use, sharing, distribution and reproduction in any medium or format, as long as you give appropriate credit to the original author(s) and the source, provide a link to the Creative Commons licence, and indicate if you modified the licensed material. You do not have permission under this licence to share adapted material derived from this article or parts of it. The images or other third party material in this article are included in the article's Creative Commons licence, unless indicated otherwise in a credit line to the material. If material is not included in the article's Creative Commons licence and your intended use is not permitted by statutory regulation or exceeds the permitted use, you will need to obtain permission directly from the copyright holder. To view a copy of this licence, visit <http://creativecommons.org/licenses/by-nc-nd/4.0/>.

© The Author(s) 2025